

# INVESTIGATION OF THE ELECTRIC-FIELD PROFILE IN MICROCRYSTALLINE SILICON P-I-N SOLAR CELLS BY CROSS-SECTIONAL SCANNING KELVIN PROBE MICROSCOPY

D. Dominé<sup>1</sup>, J. Bailat, M. Python, N. Wyrsh, C. Ballif

University of Neuchâtel, Institute of Microtechnology, Breguet 2, CH-2000 Neuchâtel, Switzerland

<sup>1</sup>Phone: (+)41 32 718 3312; Fax: (+)41 32 718 3201; E-mail: didier.domine@unine.ch

H. R. Moutinho, C.-S. Jiang, M. M. Al-Jassim

National Renewable Energy Laboratory, 1617 Cole Boulevard, Golden, Colorado 80401

**ABSTRACT:** Scanning Kelvin probe microscopy (SKPM) is performed on cross-sections of microcrystalline silicon ( $\mu\text{-Si:H}$ ) p-i-n solar cells deposited on a surface-textured ZnO layer. Cross-sections are either prepared by a simple fracture procedure or by mechanical polishing. Profiles of the variation in the electric-field induced by different bias voltage ( $V_{\text{bias}}$ ) applied to the cell are deduced from SKPM potential measurements by calculating the first derivative of the modification of the surface potential profiles. The amplitude of the  $V_{\text{bias}}$ -induced electric-field is found to be heterogeneously distributed over different  $\mu\text{-Si:H}$  clusters. From these measurements, we suggest that each cluster behaves as an "isolated nanodiode", the electric-field changes being mainly confined within  $\sim 500$  nm in the intrinsic  $\mu\text{-Si:H}$  layer either near the p-i or near the i-n interface. This supports the assumption of an important contribution of diffusion-assisted transport along the growth axis of the large crystalline nanograins observed by transmission electron microscopy (TEM) in the  $\mu\text{-Si:H}$  clusters. A comparison of SKPM images with a TEM micrograph demonstrates that cluster boundaries in the intrinsic  $\mu\text{-Si:H}$  layer can be imaged by the SKPM technique.

**Keywords:** Micro Crystalline Si, Electric-Field, Kelvin Probe

## 1 INTRODUCTION

The relative role of drift and diffusion mechanisms involved in the carrier transport in microcrystalline silicon ( $\mu\text{-Si:H}$ ) solar cells is an open question [1]. Previous voltage-capacitance and charge-collection (time of flight) experiments conducted by Wyrsh *et al.* suggested a drift controlled transport at the grain boundaries and a diffusion controlled transport inside the grains [2,3]. Information about the electric-field distribution in the intrinsic layer is decisive for the comprehension and the optimization of the carrier collection efficiency of  $\mu\text{-Si:H}$  solar cells. In this paper, we report on nanoscale measurements of surface potentials on cross-sections of  $\mu\text{-Si:H}$  cells using scanning Kelvin probe microscopy (SKPM). Recently, this technique has been applied to the analysis of thin film silicon solar cells deposited on flat substrates. Jiang *et al.* reported on SKPM measurements on fractured cross-sections of amorphous silicon (a-Si:H) n-i-p solar cells, with the application of a bias voltage ( $V_{\text{bias}}$ ) to the sample [4]. Breymesser *et al.* reported on measurements, without  $V_{\text{bias}}$ , on polished cross-sections of  $\mu\text{-Si:H}$  p-i-n cells [5].

Here we go one step further and analyze, with a  $V_{\text{bias}}$  applied to the sample during the SKPM measurement, fractured and polished cross-sections of  $\mu\text{-Si:H}$  p-i-n solar cells deposited on a surface-textured substrate.

## 2 EXPERIMENTAL

The  $\mu\text{-Si:H}$  p-i-n solar cells are prepared by VHF plasma enhanced chemical vapor deposition in a dual-chamber deposition system. The thickness of the intrinsic layer is  $1.8 \mu\text{m}$ . The cells are grown on glass coated with a surface-textured front transparent conductive oxide (TCO). The front TCO is a zinc oxide (ZnO) layer deposited by low pressure chemical vapor deposition (LPCVD). Prior to  $\mu\text{-Si:H}$  deposition, the ZnO is exposed to a surface treatment in order to remove sharp pinches and therefore increase the  $V_{\text{oc}}$  and FF value of

the solar cell [6]. The back contact is a LPCVD ZnO layer and the cell area is patterned by  $\text{SF}_6$  plasma etching ( $0.25 \text{ cm}^2$ ). The current density-voltage curves are measured using a two-source AM1.5g sun simulator (Wacom).

The cross-sections are either prepared by simple fracture of the samples using the procedure presented in ref. [7] or are prepared by grinding and mechanical polishing. Both the fractured and polished samples are electrically connected for the application of  $V_{\text{bias}}$ .

Prior to mechanical polishing, two samples are glued in sandwich configuration with epoxy. In order to allow the electrical connection of the front and back contacts, the two samples are laterally shifted before gluing. The mechanical polishing is performed using diamond lapping films with particles sizes decreasing from  $30 \mu\text{m}$  to  $0.1 \mu\text{m}$ . To minimize the height of the step between the ZnO and the  $\mu\text{-Si:H}$  layers, a final mechanical polishing using an aluminum oxide film with a grit size of  $50 \text{ nm}$  is performed, instead of the usual chemical-mechanical polishing with a suspension of colloidal silica particles.

The SKPM measurements are performed in air at the same time as non-contact atomic force microscopy topography imaging with a ThermoMicroscopes Autoprobe CP Research system. The topographic imaging is obtained using the first resonant frequency ( $\sim 60 \text{ kHz}$ ) of the cantilever while a  $20 \text{ kHz}$  ac voltage is applied to the tip for the SKPM potential measurement (see [8] for details). The surface potential measured over the multilayer stacks depends on oxidation and water adsorption effects and on surface charge trapped at surface states; this may induce different surface Fermi level pinning for the different layers of the device [9,4]. Therefore, assuming that the filling of the electronic surface states does not change with variations of the bias voltage ( $V_{\text{bias}}$ ) applied between the front and back contacts, we can calculate the potential change in the bulk as the difference of the surface potentials measured with  $V_{\text{bias}}$  and in short-circuit condition [9]. The  $V_{\text{bias}}$ -induced electric-field profiles are then calculated as the

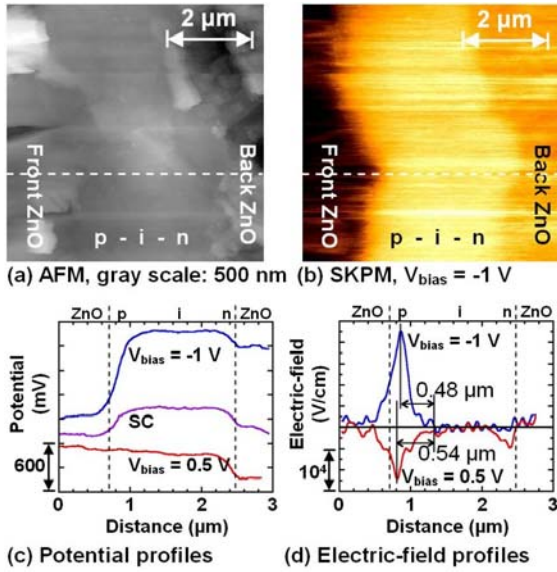


**Figure 1:** (a) AFM image and (b) the corresponding SKPM image taken under reverse-bias conditions on a fractured cross-section of a  $\mu\text{c-Si:H}$  p-i-n solar cell. (c) SKPM potential profiles measured on the dashed lines in (a) and (b), under short-circuit (SC), forward-bias ( $V_{\text{bias}} = 0.5$  V), and reverse-bias ( $V_{\text{bias}} = -1$  V) conditions. (d) Corresponding increase and decrease in electric-field induced by  $V_{\text{bias}}$ .

the first derivative of this difference [4]. A positive (negative)  $V_{\text{bias}}$  value corresponds to a forward- (reverse-) bias of the sample.

For comparison of SKPM images and transmission electron microscopy (TEM) micrographs, a solar cell is prepared by the tripod method [10] and analyzed by TEM in bright-field using a Philips CM200 microscope operated at 200 kV.

### 3 RESULTS

#### 3.1 Fractured cross-sections

Figures 1(a) and (b) show the AFM image and the corresponding SKPM image taken under reverse-bias condition, for a  $\mu\text{c-Si:H}$  solar cell, deposited on a highly surface-treated LPCVD ZnO layer, with an open-circuit voltage ( $V_{\text{oc}}$ ) of 541 mV and a fill-factor (FF) of 72.2 %. The fracture procedure produces a rough cross-section with a typical corrugation value of 200 nm. The SKPM image suffers from convolution with the topography; however, the front ZnO, the  $\mu\text{c-Si:H}$ , and the back ZnO layers can clearly be distinguished. SKPM analysis is performed in short-circuit ( $V_{\text{bias}} = 0$  V), forward-bias ( $V_{\text{bias}} = 0.5$  V) and reverse-bias ( $V_{\text{bias}} = -1$  V) conditions. The potential profiles measured on the dashed lines in Figs. 1(a) and (b) are plotted in Fig. 1(c), after averaging over 11 consecutive scan lines; the corresponding modifications of the electric-field are plotted in Fig. 1(d).

Noise in the potential profiles is amplified by the derivative procedure and produces the ripple effect visible in the field profiles in Fig. 1(d). The electric-field induced by  $V_{\text{bias}}$  is confined to the 500 first nanometers after the p-i interface. At the electrical junction, the field is increased up to a maximum value of  $2.3 \cdot 10^4$  V/cm for a  $V_{\text{bias}}$  value of -1 V (reverse-bias) and is decreased by a

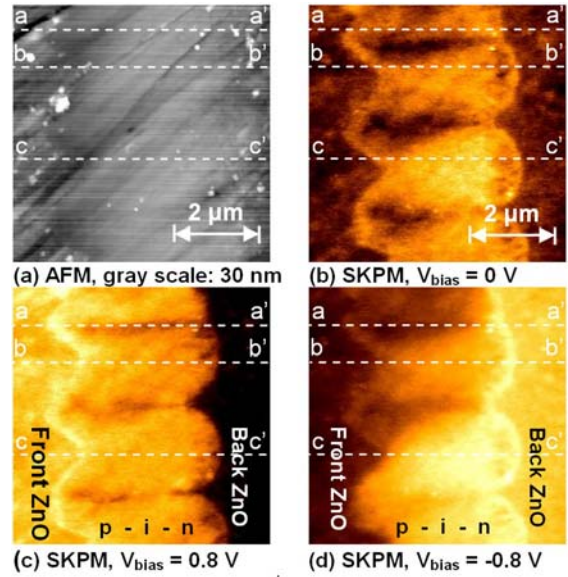


**Figure 2:** (a) AFM image and the corresponding SKPM images taken under (b) short-circuit ( $V_{\text{bias}} = 0$  V), (c) forward-bias ( $V_{\text{bias}} = 0.8$  V), and (d) reverse-bias ( $V_{\text{bias}} = -0.8$  V) conditions on a polished cross-section of a  $\mu\text{c-Si:H}$  p-i-n solar cell.

maximum value of  $-1.2 \cdot 10^4$  V/cm for a  $V_{\text{bias}}$  value of 0.5 V (forward-bias). The peak position of the electric-field profile under the  $V_{\text{bias}}$  value of -1 V is shifted 60 nm toward the bulk of the intrinsic layer, compared to the peak position under the forward-bias condition.

The apparent extension of the electric-field into the front contact is most likely due to the low spatial resolution of this measurement on a rough cross-section, as already observed for a-Si:H solar cells [4].

#### 3.2 Polished cross-section

For a polished cross-section of a  $\mu\text{c-Si:H}$  solar cell deposited on a LPCVD ZnO layer with a short surface treatment (FF = 68.3 % and  $V_{\text{oc}} = 528$  mV), Fig. 2 shows the AFM image and the corresponding SKPM images taken under short-circuit, forward-bias ( $V_{\text{bias}} = 0.8$  V) and reverse-bias ( $V_{\text{bias}} = -0.8$  V) conditions. The

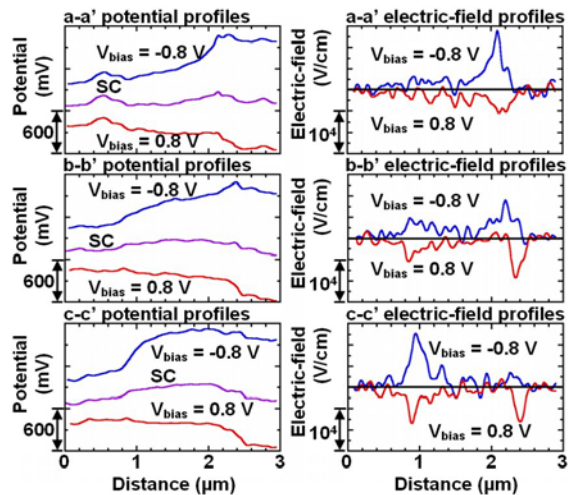


**Figure 3:** SKPM potential profiles measured on the dashed lines in Fig. 2, after averaging and the corresponding electric-field profiles induced by  $V_{\text{bias}}$ .

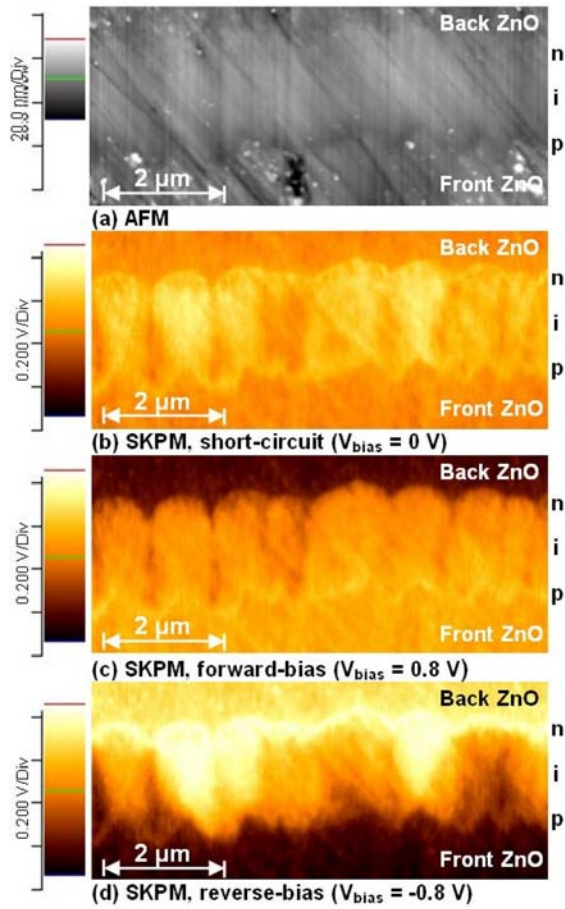


**Figure 4:** (a) AFM image and the corresponding SKPM images taken under (b) short-circuit, (c) forward-bias, and (d) reverse-bias conditions on a polished cross-section of a  $\mu\text{c-Si:H}$  p-i-n solar cell.

AFM image shows that the mechanical polishing produces scratches with a typical depth of 2 to 5 nm. The SKPM images clearly demonstrate that the  $\mu\text{c-Si:H}$  layer is actually constituted of clusters located at the peaks of the front TCO.

SKPM potential profiles measured on the dashed lines in Fig. 2 and the corresponding variations in the electric-field distribution induced by  $V_{\text{bias}}$  are plotted in Fig. 3, after averaging over 11 consecutive scan lines.  $V_{\text{bias}}$ -induced variations of the electric-field profile are in the order of  $10^4$  V/cm, mainly confined, depending on the location of the measured profile, near the p-i or near the i-n interface.

For a larger area of the same cross-section, Fig. 4 shows the AFM image and the corresponding SKPM images taken under short-circuit, forward-bias ( $V_{\text{bias}} = 0.8$  V) and reverse-bias ( $V_{\text{bias}} = -0.8$  V) conditions. The changes of the potential in the bulk for different  $\mu\text{c-Si:H}$  clusters under forward- and reverse-bias conditions are highlighted in Fig. 5, where the SKPM image taken under short-circuit (Fig. 4(b)) is subtracted from the images taken under forward-bias (Fig. 4(c)) and reverse-bias (Fig. 4(d)). The cluster boundaries visible in Figs. 2 and 4 (drops of  $\sim 150$  mV in the SKPM potential) are not visible in Fig. 5.

The gradient of the potential difference in Fig. 5 is equivalent to the  $V_{\text{bias}}$ -induced electric-field in the bulk beneath the surface of the cross-section. Under forward-

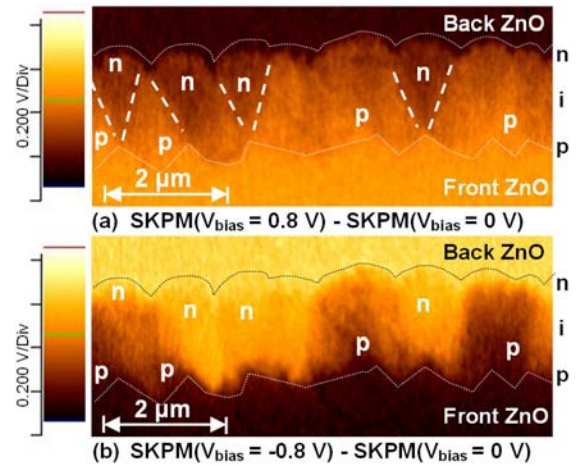


**Figure 5:** Subtraction of the SKPM image taken under short-circuit condition from the SKPM images taken under (a) forward-bias, and (b) reverse-bias conditions.

bias (Fig. 5(a)), a gradient of the potential difference is visible at the p-i interface only near some peaks of the TCO and not near the valleys. Dashed lines drawn in Fig. 5(a) suggest this behavior is related to  $\mu\text{c-Si:H}$  clusters grown at the peak of the TCO. Under reverse-bias (Fig. 5(b)), the gradient induced by  $V_{\text{bias}}$  is located mainly at the p-i interface, except for the clusters with a potential gradient at the i-n interface in forward-bias condition (Fig. 5(b)). This suggests a p-type or n-type character for the different clusters, as indicated in Fig. 5.

### 3.2 TEM analysis

Figure 6 shows a typical bright-field TEM micrograph of a  $\mu\text{c-Si:H}$  solar cell deposited on a surface-treated LPCVD ZnO layer. This micrograph clearly shows that on a surface-textured TCO, the  $\mu\text{c-Si:H}$  layer is constituted of clusters formed by columnar crystalline nanograins with sizes larger than 100 nm.

The clusters are either separated by cracks or by boundaries formed by the collision of columnar nanograins belonging to different clusters. The  $\mu\text{c-Si:H}$  material grown on the valleys of the TCO is constituted by smaller, less oriented nanograins; with a presumably smaller crystalline volume fraction.

## 4 DISCUSSION

### 4.1 Fractured cross-section

Our results show first that SKPM measurements can be performed on rough fractured cross-sections of p-i-n  $\mu\text{c-Si:H}$  solar cells deposited on surface-textured LPCVD ZnO. However, analysis of large areas is experimentally challenging due to the high corrugation of the fractured cross-section.

Moreover, due to variations of the capacitive coupling between the tip and the sample surface, the interpretation of SKPM images taken on rough cross-sections is complicated by a convolution of the measured potential with the topography. This simple preparation method allows nevertheless the measurement of the surface potential profile and the calculation of the electric-field profile on some chosen locations.

Despite of a good collection efficiency of the carriers (FF = 72.2 %), the calculated  $V_{\text{bias}}$ -induced electric-field

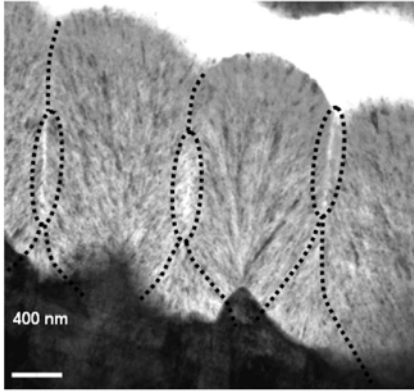


**Figure 6:** Bright-field TEM micrograph of a  $\mu\text{c-Si:H}$  p-i-n solar cell deposited on a LPCVD ZnO layer.

profile is confined to the 500 first nanometers after the p-i interface. This suggests that the intrinsic layer is slightly n-type, as observed in ref. [11] for thick a-Si:H cells. This would also indicate that a strong diffusion of carriers is possible in  $\mu\text{c-Si:H}$  intrinsic layers. However, as we measure only the modification of the electric-field we cannot evaluate the presence of an initial electric-field. Voltages drops at the p-i interface must then indicate a large interface defect density.

The peak positions of electric-field profiles correspond to the location of the electrical junction, which is different from the p-i metallurgical junction. Due to the widening of the depletion region in the “intrinsic” layer under reverse-bias condition, the electrical junction is shifted toward the bulk in reverse-bias. This explains the shift of the peak in Fig. 1(d) for the reverse-bias condition.

#### 4.2 Polished cross-section

Mechanical polishing produces a planar cross-section allowing the analysis of large areas, including many of the typical  $\mu\text{c-Si:H}$  clusters growing on surface-textured TCOs.

Both for the fractured and the polished sample, the SKPM potential profiles measured under short-circuit condition are essentially flat on the  $\mu\text{c-Si:H}$  layer. This indicates a Fermi level pinning at the surface of the cross-section for the whole thickness of the intrinsic layer, as previously observed for a-Si:H solar cells [11].

Although we cannot definitely exclude parasitic effects induced by the polishing procedure (for example heterogeneous oxide layer thickness or structure), our analysis of the SKPM potential profiles indicates that the amplitude of the electric-field modification induced by  $V_{\text{bias}}$  is heterogeneously distributed. It is mainly confined near the p-i interface for some cases and near the i-n interface for some others, and this depends strongly on the cluster considered. This gives rise to a concept of “isolated nanodiodes” with independent characteristics. We speculate that the n- or p-type character of a given cluster is conditioned by the surrounding cracks and cluster boundaries, which may have different electrical and structural characteristics. In a recent work, Python *et al.* indeed demonstrated that the effect of cracks can be modeled by diode-like shunts, with a high individual reverse saturation current, related on the length of the crack [12].

The lower SKPM potential observed at the cluster

boundaries in Figs. 2 and 4, correspond to higher local work-function. This demonstrates a local upward band bending, due to negative charges located at the boundaries. On one hand, this negative charge could be the consequence of a difference in the surface states at these defective regions, which are structurally different with porosity and probably a lower crystalline fraction. On the other hand, Nasuno *et al.* reported on an enhanced diffusion of boron in the a-Si:H matrix during the deposition of  $\mu\text{c-Si:H}$  on textured ZnO [13]. Consequently, we speculate that the negative charge of the cluster boundaries could be explained by the presence of activated boron.

The cluster boundaries visible in the surface potential images (Figs. 2 and 4) are not visible in the potential difference images (Fig. 5) because the boundaries induce mainly surface effects. Indeed, the surface potential difference produced by the application of  $V_{\text{bias}}$  is affected by the average effect in the depth equal to the depletion width in the normal direction to the surface of the cross-section.

#### 4.3 Comparison with TEM

Microstructure features highlighted in the TEM micrograph (Fig. 6) can directly be compared to the features of SKPM images presented in Figs. 2(b) and 5(a). This comparison demonstrates that cluster boundaries in the intrinsic  $\mu\text{c-Si:H}$  layer can be imaged by the SKPM technique. However, the distinction between cluster boundaries and cracks is not clear in the SKPM images.

The region of  $\mu\text{c-Si:H}$  material grown on the valleys of the TCO correspond to areas, between the clusters, visible under forward-bias condition in the SKPM image of Fig. 5(a). These areas present a p-type character and therefore, due to their supposed lower crystalline volume fraction, may be more contaminated by boron than the clusters themselves.

## 5 CONCLUSIONS

SKPM analysis can be performed on rough fractured cross-sections of  $\mu\text{c-Si:H}$  solar cells deposited on a surface textured LPCVD ZnO. However, the measured surface potential is sensitive to convolution with the topography of the fractured cross-section; this may render difficult the interpretation of features observed in the SKPM images.

Providing a mechanical polishing of the cross-section, we show that the amplitude of the modification of the electric-field induced by the bias voltage is heterogeneously distributed over different  $\mu\text{c-Si:H}$  clusters. Each cluster behaves as an “isolated nanodiode”, with the electric-field confined within  $\sim 500$  nm in the intrinsic  $\mu\text{c-Si:H}$  layer either near the p-i or near the i-n interface. This supports the assumption of an important contribution of diffusion-assisted transport along the growth axis of the large crystalline nanograins observed by TEM in the  $\mu\text{c-Si:H}$  clusters. A comparison of SKPM images with a TEM micrograph demonstrates that cluster boundaries in the intrinsic  $\mu\text{c-Si:H}$  layer can be imaged by the SKPM technique.

The electrical behavior of isolated clusters is presumably affected by their surrounding, formed of defective cluster boundaries and cracks. On the SKPM

images taken under short-circuit and forward-bias conditions, the cluster boundaries appear as areas with a low local surface potential, demonstrating a local negative charge. Possible explanations could be a selective boron contamination of the clusters boundaries or a difference in the electronic surface states filling at these defective regions.

#### ACKNOWLEDGMENTS

This work was partly supported by the Swiss Federal Energy Office (OFEN) under grant number 101191. One of the authors (D. D.) thanks the Fondation Charles-Edouard Guillaume, Switzerland, for a fellowship.

#### REFERENCES

- [1] J. Meier et al., *Appl. Phys. Lett.* 65 (1994) 860.
- [2] N. Wyrsh et al., *Mat. Res. Soc. Symp. Proc.* 507 (1998) 181.
- [3] N. Wyrsh et al., *J. Non-Crys. Solid*, Vol. 227-230(1998) 1272.
- [4] C.-S. Jiang et al., *Mat. Res. Soc. Symp. Proc.* 808 (2004) A9.42.1.
- [5] Breymesser et al., *Sol. Energy Mater. Sol. Cells* 66 (2001) 171.
- [6] Bailat et al., *Proc. of the 4th WCPEC Conf.* (2006) 1533.
- [7] C. Ballif et al., *Ultramicroscopy* 85 (2001) 61.
- [8] C.-S. Jiang et al., *J. Appl. Phys.* 89 (2001) 1418
- [9] C. Ballif et al., *J. Appl. Phys.* 89 (2001) 1418.
- [10] J. Benedict et al., *Mat. Res. Soc. Symp. Proc.* 254 (1992) 121.
- [11] C.-S. Jiang et al., *Thin Solid Films* 472 (2005) 203.
- [12] M. Python et al., *Proc. ICANS 2007.*
- [13] Y. Nasuno et al., *Appl. Phys. Lett.* 81 (2002) 3155.